Hindawi
Shock and Vibration
Volume 2022, Article ID 1057422, 11 pages
https://doi.org/10.1155/2022/1057422

Research Article

Research for Pedestrian Steel Bridge Design of Neural Network in Structural Model Updating

Rui Zhao,[1,2] Yuhang Wu ,[1] and Zehua Feng[1]

[1]*School of Civil Engineering and Architecture, Xinjiang University, Urumqi 830047, China*
[2]*Xin Jiang Key Lab of Building Structure and Earthquake Resistance, Urumqi 830047, China*

Correspondence should be addressed to Yuhang Wu; wuyh0321@stu.xju.edu.cn

Received 10 March 2022; Revised 4 April 2022; Accepted 13 April 2022; Published 2 May 2022

Academic Editor: Yonggang Zhang

The application of the neural network method in health monitoring and structural system identification has received extensive attention. A reasonable neural network structure is very important for its performance. This paper takes the pedestrian bridge of the Xingfu intersection in Urumqi, China, as the research object and uses MIDAS/Civil to establish a finite element analysis model. Taking the natural vibration frequency obtained from the dynamic test of the actual bridge as the target, two kinds of neural networks are used to predict the structural material parameters. An appropriate bridge model correction method is selected by comparing the prediction results of the BP neural network and the GRNN. The test results show that the pedestrian bridge model based on MIDAS/Civil has a high accuracy, but it still does not meet the actual needs. The modified model based on the BP neural network is close to the actual measured results, and a more accurate finite element analysis model can be established by this method, which makes the modified model closer to the real stress state of the structure.

1. Introduction

The long-term health inspection of steel structure bridge is of great significance to its safety, and the current measures to ensure the long-term safety performance of the bridge mainly focus on the inspection and reinforcement. The health monitoring and prediction of bridges are based on finite element analysis. Firstly, the measuring points are arranged at each node of the bridge, and the measured data (concrete strength, deflection value, strain value, and low-order natural frequency of the bridge) are collected. Then, the finite element model is established according to the existing design drawings and combined with external conditions. The state of the bridge is judged by the correlation analysis between the measured value and the calculated value. However, the measured results are often different from the calculated results of the bridge finite element model, and the degree of difference often determines the evaluation results of the bridge. Therefore, the establishment of a more accurate finite element model is the basis of structural analysis. Due to the discreteness degree of the finite element model, the setting of modeling parameters, some simplified assumptions are used in modeling, and the calculated values of the finite element model bring errors. In addition, the initial finite element model established strictly in accordance with the design drawings cannot actually reflect the mechanical behavior of the structure due to the influence of material performance deviation, structural degradation or damage, and other factors [1]. Therefore, it is necessary to modify the bridge finite element model according to the measured results of bridge detection to improve the accuracy and reliability of the bridge finite element model. The essence of finite element model modification is an approximation problem, and one or several indexes of the finite element model are infinitely close to the real value by modifying various parameters of the finite element model.

Using a neural network to modify the finite element model can not only reduce the calculation times but also make the predicted results tend to close the actual value [2]. This paper mainly adopts BP neural network and GRNN. BP neural network (backpropagation neural

network) is a kind of multilayer feedforward neural network. The error between the actual output and the expected output of the system is reduced by changing the connection weights among neurons, and the weights and thresholds between the hidden layer and the output layer are adjusted forward and backward according to the gradient descent method. GRNN (general regression neural network) is a feedforward neural network model based on the nonlinear regression principle. GRNN is improved based on RBF and has a similar structure. The difference lies in the addition of a summation layer and the removal of the weight connection between the hidden layer and the output layer (the least-square superposition of the Gaussian weight).

The core factor of the stability of a building structure is determined by its own material and structure. It is predicted by the neural network, which makes the model reference. Alkayem et al. [3–7] proposed that improving the accuracy of the intelligent algorithm for computing model correction is a direction worthy of study and summarized the model correction methods based on the neural network comprehensively. In 2004, Fei et al. [8–10] used RBF neural network to conduct a revision study on the aircraft model, and the results showed that the design parameter error was within 2%, and the modal frequency error was within 1%. In 2012, Wang et al. [11, 12] applied a neural network to the finite element model modification of a reinforced concrete bridge and verified that the modified finite element model could reflect the physical state of the structure more truly and better reflect the real dynamic characteristics of the bridge structure. In 2017, Jia et al. [13, 14] modeled the PC hollow beam that has been in service for more than 20 years and modified it by using a neural network intelligent algorithm. The physical state between the modified finite element model and the actual structure is very close. The elastic modulus of the steel strand is consistent with the experimental value, and all errors are controlled within 5%. In 2018, Bao et al. [15–17] used MIDAS to establish a bridge model and BP neural network to modify the model based on the deflection. The deflection error of the modified bridge finite element model was less than 10%, and a good correction effect was obtained.

Previous studies prove that neural network has a good effect on model modification, but few scholars apply a neural network to model modification of pedestrian steel bridge. In this paper, BP neural network and GRNN in radial basis neural network are used as the correction method. Urumqi Xingfu Road pedestrian bridge is taken as the model to be modified. Taking the characteristic quantity as the independent variable and the steel design parameters as the dependent variable, the neural network intelligent algorithm is used to approximate the nonlinear mapping relationship between the two [18]. Then, the generalization property of the neural network is used to solve the target value of design parameters directly. Through the reliability comparison and error analysis of BP neural network and GRNN training test results, a model modification method suitable for the pedestrian bridge was found.

Figure 1: Urumqi Xingfu Road pedestrian bridge.

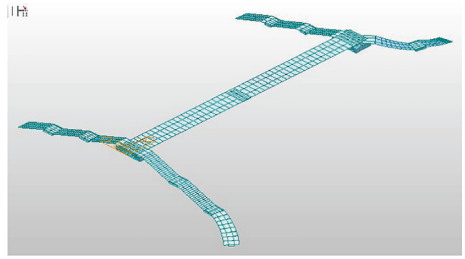

Figure 2: Finite element model of the pedestrian bridge.

2. Project Overview

Xinjiang Urumqi Xingfu Road pedestrian steel bridge was built in 2002 and is located at the intersection of the Urumqi beltway and Xingfu Road in Urumqi, China, as shown in Figure 1. The main pedestrian bridge has a net height of 5 m and a span of 23.763 m and 25.762 m, respectively. The main girder adopts a uniform cross-section single-cell box girder structure, which is 1 m high and 4 m wide, and the thickness of the roof is 10 mm, the thickness of the bottom plate is 16 mm, the thickness of the web is 12 mm, and the box girder internal welding 10 mm thick stiffening ribs. The bridge is equipped with 4 escalators, which are welded with the main beam. The width of the staircase is 2.5 m, and the height-width ratio of the steps is 1 : 3. The ladder beams are all steel box girder structure, with a height of 280 mm and the plate thickness of 10 mm. The piers are made of hot-rolled seamless steel tubes, with a wall thickness of 16 mm and a diameter of 426 mm. The foundation is an expanded concrete foundation, the balustrade is a carbon stainless steel composite steel pipe, and the bridge deck pavement adopts a 15 mm thick rubber plate; Q235B killed steel is used for the pier column and main beam steel plate, and Q235C killed steel is used for other members. The main components are welded in the factory and then transported to the site for welding and assembly.

3. Model Establishment and Dynamic Test

3.1. Initial Model Establishment. According to the design drawing size of the pedestrian bridge, the finite element model of the pedestrian steel bridge is established by using MIDAS/Civil. Semirigid rubber bearings were set for the main beam, escalator beam, and column of the pedestrian bridge, and consolidation boundary conditions were

Table 1: Calculation table of the first five natural vibration frequencies of the pedestrian bridge.

Order	First order	Second order	Third order	Fourth order	Fifth order
Frequency (Hz)	4.4668	5.5481	6.2427	8.1857	10.4471

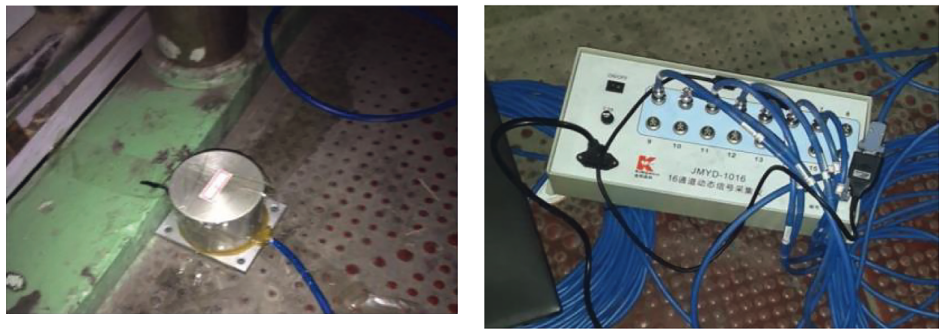

(a) (b)

Figure 3: Dynamic test instrument. (a) Acceleration vibration pickup. (b) Dynamic information acquisition instrument.

selected for the supports and top pillar. Mechanical properties of materials refer to Q235 steel in the General Specifications for Design of Highway Bridges and Culverts [19] (D60-2015). The finite element model is shown in Figure 2.

The dynamic characteristics of the pedestrian bridge model were analyzed by using the subspace iteration method. The first 5-order natural vibration frequencies of the pedestrian bridge are calculated as shown in Table 1.

According to the study of Fan et al. [20, 21], the walking frequency of human is 2~4 Hz, and the first 2 vibration modes of the bridge need only be considered in model modification and dynamic test of the real bridge for the pedestrian bridge.

3.2. Self-Vibration Characteristics Test. The test was conducted in the early morning in order to minimize the influence of external factors such as the stream of people and vehicles on the dynamic test results. JMC2-2091 acceleration-type vibration pickup and JMYD-1016 dynamic information acquisition instrument from Jinma High-tech Institute Changsha China were used. The acceleration-type vibration pickup is fixed at each measuring point to record the acceleration waveform when the pedestrian bridge vibrates. It is connected to the dynamic information acquisition instrument through the cable, and the acceleration signal is amplified, recorded, and analyzed. Finally, the acceleration signal is connected to a laptop computer and stored on a disk for spectrum analysis (Figure 3).

11 measuring points are selected in this dynamic test, and the layout is shown in Figure 4. Cylindrical semirigid rubber bearing is set on the top of the column, it is considered that no displacement occurs at this point, so no measuring point is set on the top of the column. The test was divided into two groups, and the first group was the measuring points 1-1 to 1-7 (Figure 4). In order to connect the test data of the two groups, position 1-7 of the first group was kept unchanged as the position 2-7 of the second group. The test system is shown in Figure 5.

DASP software was used to analyze the measured data after the test [22, 23]. DASP software shows that the first-order vertical natural vibration frequency obtained from the dynamic test of the pedestrian bridge is 4.9804 Hz, and the second-order vertical natural vibration frequency is 5.9765 Hz. There is some error between the test results and the finite element calculation results.

It can be seen from Table 2 that the maximum error of the initial model of the pedestrian bridge established by MIDAS/Civil is only 10% in strict accordance with the design drawings, which has high accuracy. The initial model error is small, the degradation of material properties causes the error, and the parameters of materials in the structure can be predicted using neural networks [24, 25].

4. Determine the Correction Parameters

4.1. Factors Affecting Natural Vibration Frequency. According to equations (1) and (2) for the approximate solution of the natural vibration frequency of the structure by the energy method given in the study of Ye et al. [26–28], the influencing factors of the natural vibration frequency of the structure can be determined.

$$\omega^2 = \frac{\int_0^1 EI\left[Y''(x)\right]^2}{\int_0^1 \overline{m}(x)\left[Y(x)^2 dx + \sum m_i Y_i^2\right]}, \tag{1}$$

$$f = \frac{\omega}{2\pi}, \tag{2}$$

where f is the frequency; ω is the circular frequency; E is the elastic modulus of material; I is the section moment of inertia; $Y(x)$ is the sectional shape function; Y_i is the amplitude of the particle m_i; m is the weight; l is the structural span.

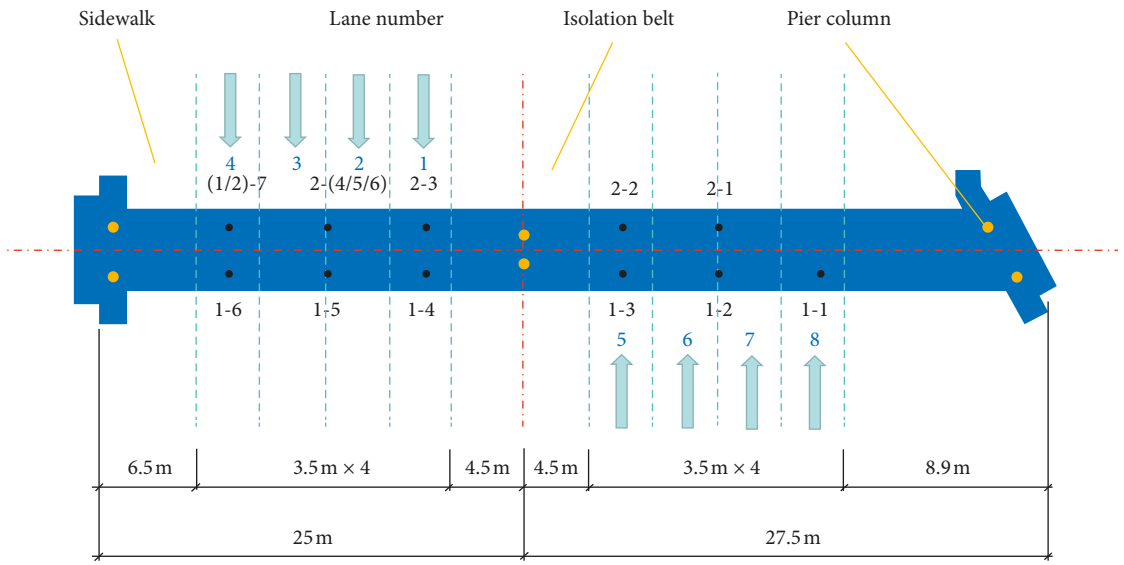

Figure 4: Layout of pedestrian bridge dynamic test points.

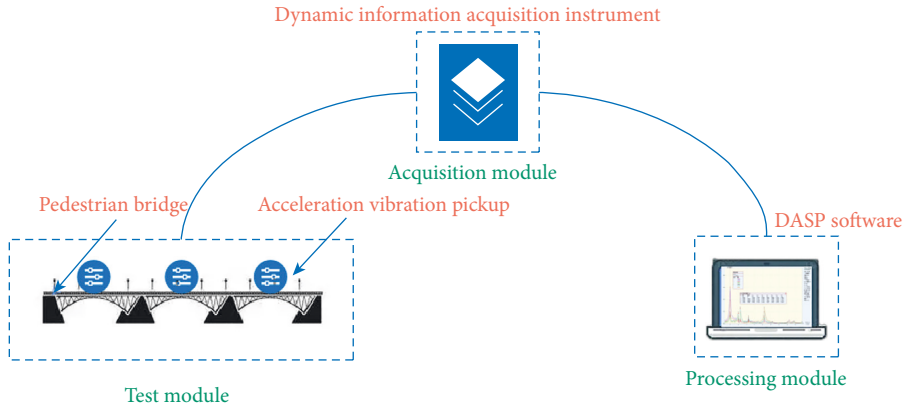

Figure 5: Self-vibration test system.

Table 2: Comparison table of test results and calculation results.

Order	Test results (Hz)	Calculation result (Hz)	Error (Hz)	Relative error (%)
First order	4.9804	4.4668	0.5136	10.3
Second order	5.9765	5.5481	0.4284	7.16

The natural vibration frequency of the structure is related to the elastic modulus of the material, sectional structure, material density, and the structural form of the bridge according to (1) and (2). According to the size, shape, weight, and allowable deviation of hot-rolled steel plate and strip [29, 30], a certain size deviation is allowed in the actual production process of components. The elastic modulus and density of components are the same, and the specific range is shown in Table 3.

4.2. Sensitivity Analysis of Influencing Factors. The sensitivity of candidate parameters should be identified first, and insensitive factors should be eliminated when selecting correction parameters. Because the nonsensitive coefficient has no obvious correction result to the model during the correction, the correction has little significance. Therefore, the model should be modified by modifying the sensitivity coefficient.

Figure 6 shows that the elastic modulus and density of materials are the main factors affecting the natural vibration frequency of structures. The sensitivity of the same parameter is not the same under different vibration modes. If only one mode is used as the correction target, the model modification will cause a certain deviation from the rest modes. Therefore, different vibration modes of the model to be modified should be taken as the correction target at the same time. In the first- and second-order cases, the elastic

Table 3: Allowable range of material ex-factory performance.

Specification range	Thickness of steel plate H (mm)	Elastic modulus E (Pa)	Material densityρ (kg/m^3)
Upper limit	$H+1$	1.9×10^{11}	7800
Lower limit	$H-1$	2.1×10^{11}	8000

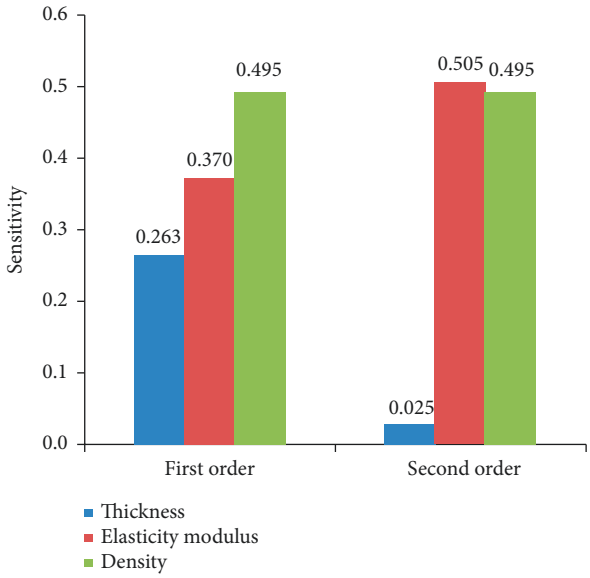

Figure 6: Sensitivity analysis of candidate parameters.

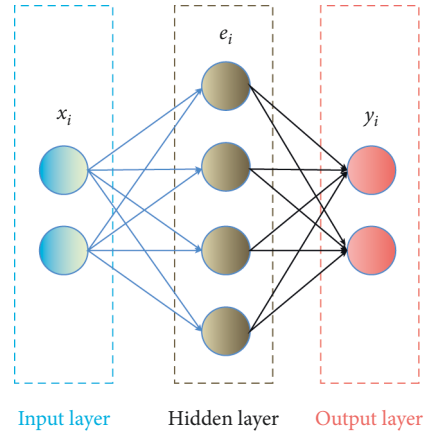

Figure 7: Working principle of the neural network.

modulus and density of the material are still the main factors affecting the natural vibration frequency of the structure. Hence, the elastic modulus and density of the material can be used as the variables of model modification to modify the first- and second-order modes simultaneously.

5. Construct Neural Network

5.1. Sample Selection. A neural network algorithm mainly simulates the neural structure and working principle of biology to carry out mathematical modeling of the complex mapping relationship between input and output values [31]. Using a neural network to modify the computational model can not only avoid the iterative solution based on inverse problem model modification but also avoid the uncertainty and complexity of nonlinear optimization. The input layer, hidden layer, and output layer together constitute the basic structure of the neural network, and its working principle is shown in Figure 7.

It is the set of right samples that are needed to provide for network optimization when you are building a neural network. The optimization process is to compare the calculated output value with the input sample value and then adjust the weight and threshold value under the training of learning rules to make the model output close to the sample value [32–34]. Sample selection was carried out in combination with the modified parameters selected in Section 3.2 and the material performance interval in Table 3. 10 equal parts are divided according to the difference between upper and lower limits of parameters; that is, each sample value increases the difference by 10% compared with the last sample. This gives 11 values for each correction parameter; the 2 parameters of the model and 11 values of each parameter can be regarded as a common combination of all parameters of a test (112 times). Sample selection is shown in Table 4.

Table 4: Sample selection table.

Order	Elasticity modulus E (Pa)	Material density ρ (kg/m^3)
1	1.9×10^{11}	7800
2	1.92×10^{11}	7820
3	1.94×10^{11}	7840
4	1.96×10^{11}	7860
5	1.98×10^{11}	7880
6	2.0×10^{11}	7900
7	2.02×10^{11}	7920
8	2.04×10^{11}	7940
9	2.06×10^{11}	7960
10	2.08×10^{11}	7980
11	2.1×10^{11}	8000

The 121 training samples were divided into two parts, 111 training sets and 10 test sets, respectively. All samples were selected according to the principle of randomness in order to ensure the reliability of network training.

5.2. BP Neural Network. As a basic multilayer forward neural network, BP neural network has one input layer and one output layer. There are several hidden layers between the input and output layers, each adopts full connection mode, and the neurons of the same layer are independent [35, 36]. The neurons of the hidden layer adopt the S-type function and linear transfer function in the output layer. A three-layer neural network with a hidden layer can approximate any

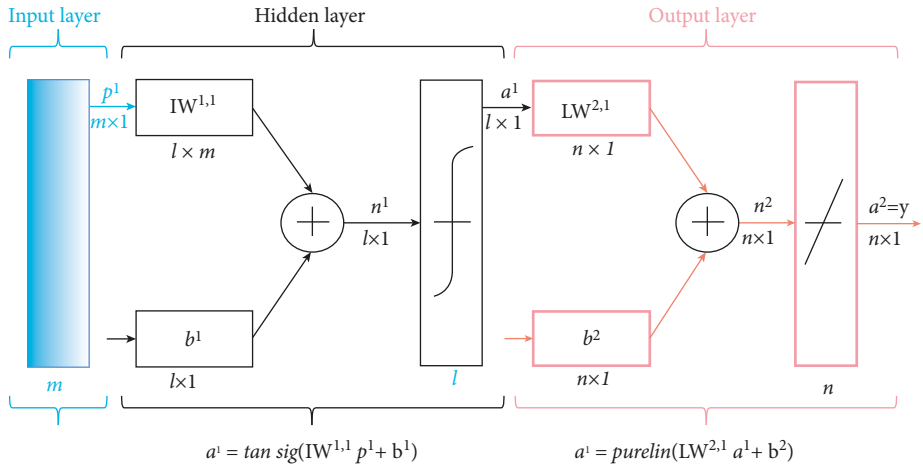

Figure 8: Structure of BP neural network.

Table 5: Test results of BP neural network.

Order	Theoretical value		Predicted value	
	Density ρ (N/m^3)	Elastic modulus E (Pa)	Density ρ (N/m^3)	Elastic modulus E (Pa)
1	7.800×10^4	1.940×10^{11}	7.807×10^4	1.943×10^{11}
2	7.860×10^4	2.000×10^{11}	7.867×10^4	2.002×10^{11}
3	7.940×10^4	2.060×10^{11}	7.938×10^4	2.059×10^{11}
4	7.880×10^4	1.960×10^{11}	7.879×10^4	1.962×10^{11}
5	7.900×10^4	2.100×10^{11}	7.895×10^4	2.099×10^{11}
6	7.840×10^4	1.980×10^{11}	7.848×10^4	1.982×10^{11}
7	7.960×10^4	1.960×10^{11}	7.974×10^4	1.963×10^{11}
8	7.860×10^4	2.020×10^{11}	7.867×10^4	2.023×10^{11}
9	7.940×10^4	2.100×10^{11}	7.939×10^4	2.100×10^{11}
10	7.920×10^4	1.980×10^{11}	7.919×10^4	1.983×10^{11}

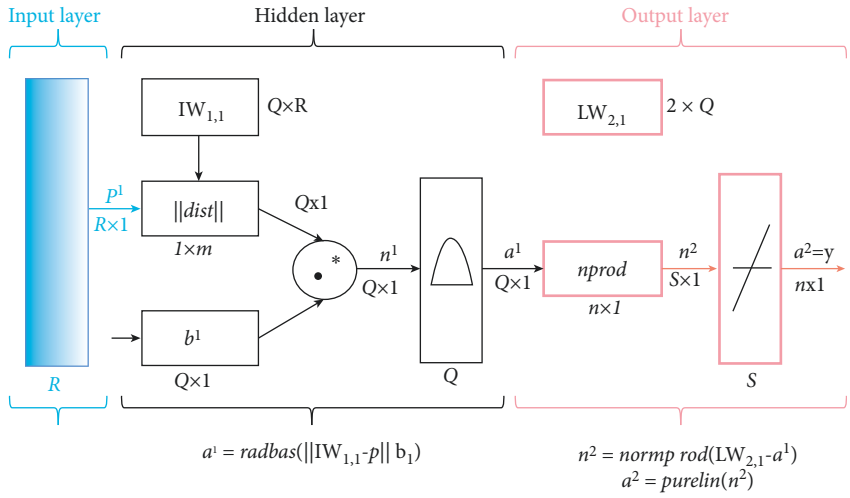

Figure 9: Structure of GRNN.

nonlinear function theoretically [37, 38]. BP neural network correction adopts an error backpropagation algorithm, which takes the weight and threshold as the cause of the error and apportions the error to the weight and threshold of each neuron through backpropagation algorithm, as shown in Figure 8. There are m neurons in the input layer, l neurons in the hidden layer, and n neurons in the output layer. The hidden layer adopts the S-type transfer function *tansig*, and

Table 6: Test results of GRNN.

Order	Theoretical value		Predicted value	
	Density ρ (N/m^3)	Elastic modulus E (Pa)	Density ρ (N/m^3)	Elastic modulus E (Pa)
1	7.800×10^4	1.940×10^{11}	7.801×10^4	1.937×10^{11}
2	7.860×10^4	2.000×10^{11}	7.861×10^4	1.999×10^{11}
3	7.940×10^4	2.060×10^{11}	7.941×10^4	2.071×10^{11}
4	7.880×10^4	1.960×10^{11}	7.890×10^4	1.959×10^{11}
5	7.900×10^4	2.100×10^{11}	7.901×10^4	2.101×10^{11}
6	7.840×10^4	1.980×10^{11}	7.839×10^4	1.979×10^{11}
7	7.960×10^4	1.960×10^{11}	7.951×10^4	1.958×10^{11}
8	7.860×10^4	2.020×10^{11}	7.871×10^4	2.020×10^{11}
9	7.940×10^4	2.100×10^{11}	7.921×10^4	2.080×10^{11}
10	7.920×10^4	1.980×10^{11}	7.891×10^4	1.999×10^{11}

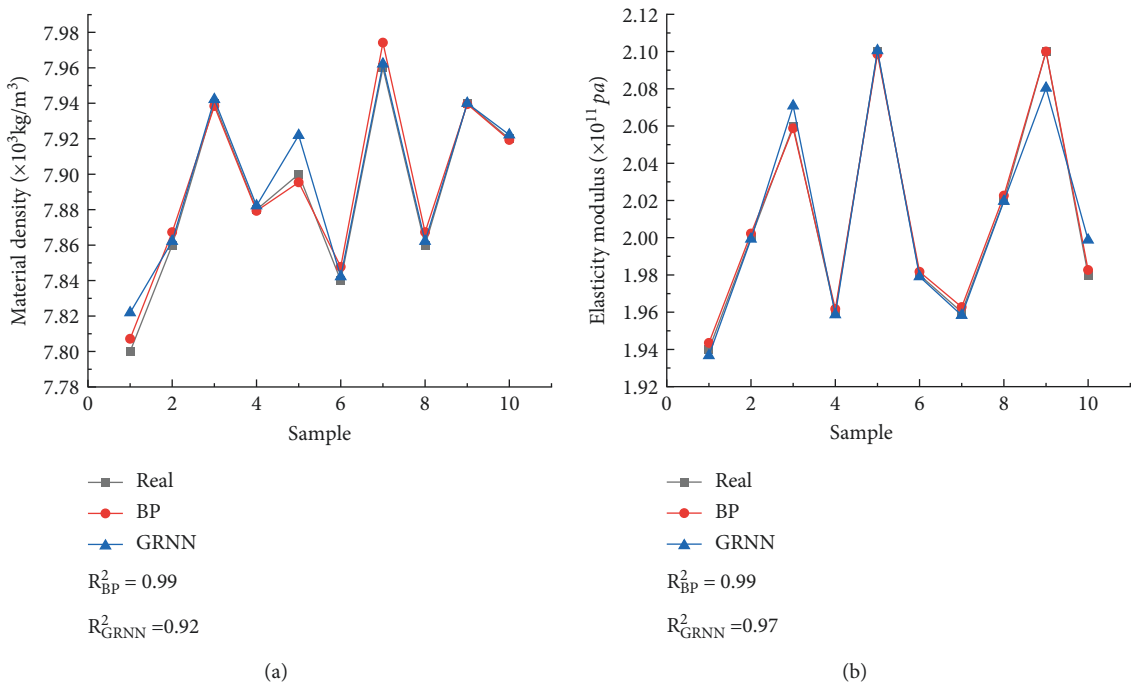

Figure 10: Reliability of neural network. (a) Density prediction reliability. (b) Reliability of elastic modulus prediction.

the output layer adopts the linear function *purelin*. According to statistics, about 75% of neural networks are derived from BP neural network [39, 40], and BP neural network is considered to be a relatively reliable neural network.

BP neural network can be created by calling the *newff* function in MATLAB neural network toolbox. The test results after training are shown in Table 5.

5.3. GRNN. GRNN, also known as a generalized neural network, is a feedforward neural network model based on the nonlinear regression principle. The structure of the GRNN is shown in Figure 9 [41, 42]. The input layer of the GRNN only sends samples into the hidden layer, and the number of neurons in the hidden layer is the same as the number of samples in the training set [43, 44]. In the hidden layer, the weight can be expressed by the Euclidean distance function II*dist*II, and the radial basis function can be expressed by the Gaussian function. The output layer adopts linear output, and its weight function adopts normalized dot product weight function *nprod*. At last, the calculation network vector n^2 is provided to the line transfer function *purlin* to obtain the calculation result [45, 46]. GRNN has the advantages of simple structure, simple training, and fast learning convergence.

GRNNs can be created by calling the MATLAB neural network toolbox *newgrnn* function. The test results after training are shown in Table 6.

5.4. Reliability Evaluation. The test results of the two neural networks are all good through the preliminary judgment [47, 48]. The relative error E_i, relative error variance S^2, and determination coefficient R^2 of test samples were selected to evaluate the reliability and error analysis of the two neural

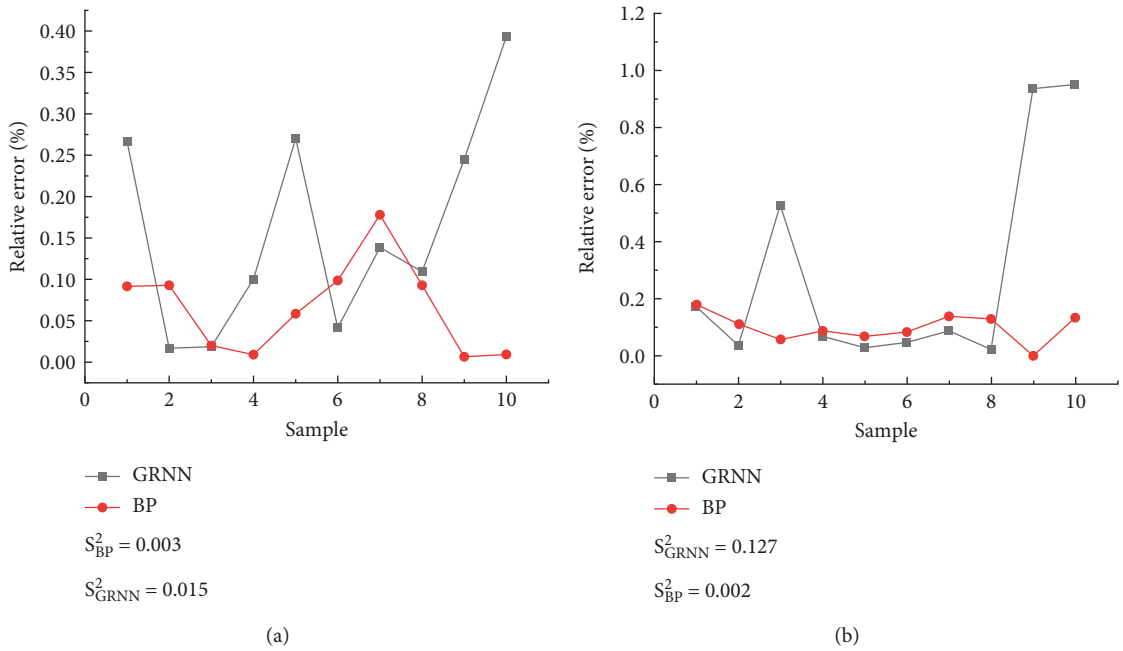

Figure 11: Relative error analysis. (a) Density relative error. (b) Relative error of elastic modulus.

Table 7: Comparison of corrected errors.

Order	Test result (Hz)	Calculation result (Hz)	Relative error (%)	Correction results (Hz)	Relative error (%)	Correction value (%)
First order	4.9804	4.4668	10.3	4.6317	7.5	2.8
Second order	5.9765	5.5481	7.16	5.7716	3.6	3.56

networks [49, 50]. The calculation methods of each coefficient are shown in equations (3)–(5), respectively.

$$E_i = \frac{|Y_i - y_i|}{y_i}, \tag{3}$$

$$S^2 = \frac{\sum_{i=1}^{n} \left(E_i - \acute{E_i}\right)^2}{n-1}, \tag{4}$$

$$R^2 = \frac{\left(n\sum_{i=1}^{n} Y_i y_i - \sum_{i=1}^{n} Y_i \sum_{i=1}^{n} y_i\right)}{\left(n\sum_{i=1}^{n} Y_i^2 - \left(\sum_{i=1}^{n} Y_I\right)^2 \left(n\sum_{i=1}^{n} y_i^2\right) - \left(\sum_{i=1}^{n} y_i^2\right)\right)}, \tag{5}$$

where Y_i $(i = 1, 2, \cdots, n)$ is the predicted value of the sample i; Y_i $(i = 1, 2, \cdots, n)$ is the theoretical value of the sample i; n is the total number of samples.

The prediction of density and elastic modulus by the neural network is shown in Figure 10, where the abscissa is the sample ordinal number, and the ordinate is density and elastic modulus, respectively [51, 52].

Figure 10 shows that the prediction curves of the two neural networks have a good coincidence with the real value curves. This indicates that the predicted value is very close to the real value, which proves that BP neural network and GRNN achieve good prediction results in density and elastic modulus. In terms of reliability, the R^2 values of the BP neural network in density and elastic modulus prediction are 0.99, and the GRNN is 0.92 and 0.97, respectively, which indicates the reliability of the BP neural network is better than GRNN in model modification [53, 54].

Relative error and relative error value variance are calculated from (3) and (4), as shown in Figure 11.

As can be seen from Figure 11, in terms of model modification and prediction, BP neural network has better stability than GRNN, and the amplitude and incidence of mutation are also smaller.

The reliability and error fluctuation of the BP neural network in the model modification are better than that of the GRNN after comparison, which BP neural network model is better used to modify the pedestrian bridge. Using BP neural network, the predicted material density and elastic modulus are $\rho = 7.84 \times 10^4 \text{N/m}^3$ and $E = 2.15 \times 10^{11}\text{Pa}$, respectively. The results are shown in Table 7.

6. Conclusion

In this paper, the dynamic characteristics of the pedestrian bridge in Urumqi China were tested to obtain the dynamic parameters of the bridge, and the neural network was used to

modify the pedestrian bridge model established by MIDAS/Civil. The following conclusions are drawn.

(1) The pedestrian bridge model established by MIDAS/Civil has high accuracy, which is found by comparing the dynamic test results with the calculation results of the initial finite element model. The degraded material parameters can be simulated by the neural network, so that the simulation results can more truly reflect the actual stress state of the structure.

(2) Through the calculation formula of natural vibration frequency, the factors affecting the natural vibration frequency of the structure are as follows: the dimensions, elastic modulus, and density of the material. The sensitivity analysis shows that the elastic modulus and material density have the greatest influence on the natural vibration frequency of the structure. The sensitivity of the same material is different in each order natural frequency.

(3) Based on reliability analysis and error analysis of calculation results of the BP neural network and GRNN, it can be seen that the two neural networks have a good effect on model modification, but the BP neural network has better reliability and smaller error fluctuation in model modification. BP neural network can be used to modify the structure model, and the modified model is closer to the real stress state of the structure.

Data Availability

The data used to support the findings of the study are included within the article.

Conflicts of Interest

The authors declare that the research was conducted in the absence of any commercial or financial relationships that could be construed as potential conflicts of interest.

Acknowledgments

This work was supported by the Xinjiang University and Xin Jiang Key Lab of Building Structure and Earthquake Resistance (XJDX1703).

References

[1] Z. Fang, G. G. Zhang, S. H. Tang, and S. J. Chen, "Finite element modeling and model updating of concrete cable-stayed bridge," *China Journal of Highway and Transport*, vol. 26, no. 3, pp. 77–85, 2013.

[2] Y. G. Zhang, J. Tang, Y. M. Cheng et al., "Prediction of landslide displacement with dynamic features using intelligent approaches," *International Journal of Mining Science and Technology*, vol. 2, no. 1, p. 111, 2022.

[3] N. F. Alkayem, M. Cao, Y. Zhang, M. Bayat, and Z. Su, "Structural damage detection using finite element model updating with evolutionary algorithms: a survey," *Neural Computing & Applications*, vol. 30, no. 2, pp. 389–411, 2018.

[4] D. Karaboga and B. Basturk, "A powerful and efficient algorithm for numerical function optimization: artificial bee colony (ABC) algorithm," *Journal of Global Optimization*, vol. 39, no. 3, pp. 459–471, 2007.

[5] M. I. Friswell and J. E. Mottershead, *Finite Element Model Updating in Structural Dynamics*, Springer, New York, NY, USA, 1995.

[6] Y. J. Yan, L. Cheng, Z. Y. Wu, and L. H. Yam, "Development in vibration-based structural damage detection technique," *Mechanical Systems and Signal Processing*, vol. 21, no. 5, pp. 2198–2211, 2007.

[7] T. Marwala, "Finite element model updating using computational intelligence techniques," *Spring*, vol. 511, no. 1, pp. 147–158, 201.

[8] Q. G. Fei and L. M. Zhang, "Finite element model updating using radial basis function neural network," *Journal of Nanjing University of Aeronautics & Astronautics*, vol. 36, no. 6, pp. 748–752, 2004.

[9] D. S. Shan, D. H. Ding, Q. Li, and H. Zhen, "Finite Element Model Updating of Single Pylon cable-stayed Bridges Based on RBF-ANN," *Journal of Chongqing Jiaotong University*, vol. 32, no. 4, pp. 555–559, 2013.

[10] W. L. Qu, D. M. Tan, and Q. Wang, "Finite element model correction of large space truss structure based on neural net," *Earthquake Engineering and Engineering Vibration*, vol. 23, no. 4, pp. 83–89, 2003.

[11] L. Wang, S. Yu, B. B. Li, and J. Ou, "Bridge model updating based on radial basis function neural network," *China Civil Engineering Journal*, vol. 45, no. S2, pp. 11–15, 2012.

[12] F. Han, D. W. Zhong, and J. Wang, "Model updating based on radial basis function neural network," *Journal of Wuhan University of Science and Technology (Natural Science Edition)*, vol. 34, no. 2, pp. 115–118, 2011.

[13] Y. M. Jia, K. Q. Guo, and X. Zhao, "Finite element model updating of the pc hollow slab beam in service of 20 years," *Science Technology and Engineering*, vol. 17, no. 26, pp. 109–111, 2017.

[14] Y. M. Jia, J. L. LiU, X. J. Liu, and L. Tang, "Vibration frequency correction of special-shaped continuous beam bridge," *Journal of China & Foreign Highway*, vol. 35, no. 4, pp. 150–153, 2015.

[15] L. S. Bao, X. Qi, and L. Yu, "Bridge finite element model correction based on BP neural network," *Journal of Highway and Transportation Research and Development*, vol. 14, no. 3, pp. 182–186, 2018.

[16] X. Y. Zeng and L. Wang, "Finite element model updating of a truss based on Optimized Neural Network," *Journal of Jiangsu University of Science and Technology*, vol. 31, no. 2, pp. 237–240, 2017.

[17] S. M. Seyedpoor, "A two stage method for structural damage detection using a modal strain energy based index and particle swarm optimization," *International Journal of Non-linear Mechanics*, vol. 47, no. 1, pp. 1–8, 2012.

[18] L. Cheng, J. Liu, Yi. Ren, and Y. Liao, "Study on very long-term creep tests and nonlinear creep-damage constitutive model of salt rock," *International Journal of Rock Mechanics and Mining Sciences*, vol. 146, Article ID 104873, 2021.

[19] Y. G. Zhang and R. Zhao, "Research of model group updating method based on frequency,NMD and modal flexibility input for steel footbridge structures," *Building Structure*, vol. 10, no. 1, pp. 31–35, 2013.

[20] M. Fang and Y. M. Luo, "Study on vibration test of urban pedestrian overpass," *Journal of Southeast University*, vol. 31, no. 5A, pp. 98–100, 2001.

[21] G. H. Zhang and Y. J. Ge, "Vibration characteristics test and analysis of concrete box girder continuous pedestrian bridge," *Journal of Vibration and Shock*, vol. 28, no. 2, pp. 102–106, 2009.

[22] D. Pan, K. Hong, H. Fu et al., "Numerical Simulation of Nanosilica Sol Grouting for Deep Tunnels Based on the Multifield Coupling Mechanism," *Geofluids*, vol. 2021, Article ID 3963291, 14 pages, 2021.

[23] L. Li, M. Zheng, X. Liu et al., "Numerical analysis of the cyclic loading behavior of monopile and hybrid pile foundation," *Computers and Geotechnics*, vol. 144, no. 6, Article ID 104635, 2022.

[24] X. S. Guo, T. K. Nian, D. Wang, and Z. D. Gu, "Evaluation of undrained shear strength of surficial marine clays using ball penetration-based CFD modelling," *Acta Geotechnica*, vol. 9, no. 1, pp. 51–60, 2021.

[25] X. Guo, T. Nian, W. Zhao et al., "Centrifuge experiment on the penetration test for evaluating undrained strength of deep-sea surface soils," *International Journal of Mining Science and Technology*, vol. 32, no. 2, pp. 363–373, 2022.

[26] T. Ye, Y. P. Li, and H. B. Xiao, "Influencing factor and analysis of natural vibration frequency of steel structural footbridge," *Urban Roads,Bridges & Flood Control*, vol. 2, pp. 48–50, 2021.

[27] S. Ivanovi, A. Pavic, and P. Reynolds, "Vibration serviceability of footbridges under human-induced excitation: a literature review," *Journal of Sound and Vibration*, vol. 279, no. 1-2, 2005.

[28] L. M. Sun and X. F. Yan, "Human walking induced footbridge vibration and its serviceability design," *Journal of Tongji University*, vol. 32, no. 8, pp. 996–999, 2005.

[29] Z. H. Zong and Z. H. Xia, "Finite element model updating method of bridge combined modal flexibility and static displacement," *China Journal of Highway and Transport*, vol. 6, no. 1, pp. 43–49, 2008.

[30] D. Pan, K. Hong, H. Fu, J. Zhou, and N. Zhang, "Experimental study of the mechanism of grouting colloidal nano-silica in over-broken coal mass," *The Quarterly Journal of Engineering Geology and Hydrogeology*, vol. 54, no. 4, Article ID qjegh2020, 161 pages, 2021.

[31] Z. H. Zhou and S. F. Chen, "Neural network ensemble," *Chinese Journal of Computers*, vol. 25, no. 1, pp. 1–8, 2002.

[32] K. L. Zhou, *Neural Network Model and its MATLAB Simulation Program Design*, Tsinghua University Press, Beijing, China, 2005.

[33] N. Srivastava, G. Hinton, A. Krizhevsky, I. Sutskever, and R. Salakhutdinov, "Dropout: a simple way to prevent neural networks from overfitting," *Journal of Machine Learning Research*, vol. 15, no. 1, pp. 1929–1958, 2014.

[34] G. Hinton, L. Deng, D. Yu et al., "Deep neural networks for acoustic modeling in speech recognition: the shared views of four research groups," *IEEE Signal Processing Magazine*, vol. 29, no. 6, pp. 82–97, 2012.

[35] P. Li, L. K. Zeng, A. Z. Shui, and J. X. L. Y. W. Hui, "Design of forecast system of back propagation neural network based on matlab," *Computer Applications and Software*, vol. 25, no. 4, pp. 149-150, 2008.

[36] S. Ding, C. Su, and J. Yu, "An optimizing BP neural network algorithm based on genetic algorithm," *Artificial Intelligence Review*, vol. 36, no. 2, pp. 153–162, 2011.

[37] W. Shen, G. Shi, Y. Wang, J. Bai, R. Zhang, and X. Wang, "Tomography of the dynamic stress coefficient for stress wave prediction in sedimentary rock layer under the mining additional stress," *International Journal of Mining Science and Technology*, vol. 31, no. 4, pp. 653–663, 2021.

[38] X. Kong, S. Li, E. Wang et al., "Experimental and numerical investigations on dynamic mechanical responses and failure process of gas-bearing coal under impact load," *Soil Dynamics and Earthquake Engineering*, vol. 142, Article ID 106579, 2021.

[39] Z. Li, X. Zhang, Y. Wei, and M. Ali, "Experimental study of electric potential response characteristics of different lithological samples subject to uniaxial loading," *Rock Mechanics and Rock Engineering*, vol. 54, no. 1, pp. 397–408, 2021.

[40] J. Ma, X. Li, J. Wang et al., "Experimental study on vibration reduction technology of hole-by-hole presplitting blasting," *Geofluids*, 2021.

[41] X. Li, Z. Cao, and Y. Xu, "Characteristics and trends of coal mine safety development," *Energy Sources, Part A: Recovery, Utilization, and Environmental Effects*, vol. 12, no. 1, pp. 1–19, 2020.

[42] Y. Niu, E. Wang, Z. Li et al., "Identification of Coal and Gas Outburst-Hazardous Zones by Electric Potential Inversion during Mining Process in Deep Coal Seam," *Rock Mech Rock Eng*, vol. 2, no. 6, pp. 121–129, 2022.

[43] K. S. Keem Siah Yap, C. P. Chee Peng Lim, and I. Z. Abidi, "A hybrid ART-GRNN online learning neural network with a ε-Insensitive loss function," *IEEE Transactions on Neural Networks*, vol. 19, no. 9, pp. 1641–1646, 2008.

[44] F. Frost and V. Karri, "Performance Comparison of BP and GRNN Models of the Neural Network Paradigm Using a Practical Industrial Application," in *Proceedings of the International Conference on Neural Information Processing IEEE*, Perth, WA, Australia, November 2002.

[45] S. Liu, X. Li, D. Wang, and D. Zhang, "Investigations on the mechanism of the microstructural evolution of different coal ranks under liquid nitrogen cold soaking," *Energy Sources, Part A: Recovery, Utilization, and Environmental Effects*, vol. 7, no. 1, pp. 1–17, 2020.

[46] X. Kong, D. He, X. Liu et al., "Strain characteristics and energy dissipation laws of gas-bearing coal during impact fracture process," *Inside Energy*, vol. 242, Article ID 123028, 2022.

[47] H. Wu, G.-y. Zhao, and S.-w. Ma, "Failure behavior of horseshoe-shaped tunnel in hard rock under high stress: phenomenon and mechanisms," *Transactions of Nonferrous Metals Society of China*, vol. 32, no. 2, pp. 639–656, 2022.

[48] X. L. Li, S. J. Chen, and S. Wang, "Study on in situ stress distribution law of the deep mine taking Linyi Mining area as an example," *Advances in Materials Science and Engineering*, vol. 9, no. 4, Article ID 5594181, 2021.

[49] X. L. Li, S. J. Chen, Q. M. Zhang, X. Gao, and F. Feng, "Research on theory, simulation and measurement of stress behavior under regenerated roof condition," *Geomechanics and Engineering*, vol. 26, no. 1, pp. 49–61, 2021.

[50] X.-l. Li, S.-j. Chen, S.-m. Liu, and Z.-h. Li, "AE waveform characteristics of rock mass under uniaxial loading based on Hilbert-Huang transform," *Journal of Central South University*, vol. 28, no. 6, pp. 1843–1856, 2021.

[51] J. Wang, T. Zuo, X. Li, Z. Tao, and J. Ma, "Study on the fractal characteristics of the pomegranate biotite schist under impact loading," *Geofluids*, 2021.

[52] D. Pan, K. Hong, H. Fu, J. Zhou, N. Zhang, and G. Lu, "Influence characteristics and mechanism of fragmental size of broken coal mass on the injection regularity of silica sol

grouting," *Construction and Building Materials*, vol. 269, Article ID 121251, 2021.

[53] G. Han, Yu. Zhou, R. Liu, Q. Tang, X. Wang, and L. Song, "Infuence of surface roughness on shear behaviors of rock joints under constant normal load and stifness boundary conditions," *Natural Hazards*, vol. 2, pp. 1–18, 2022.

[54] M. He, Z. Zhang, J. Zhu, N. Li, G. Li, and Y. Chen, "Correlation between the rockburst proneness and friction characteristics of rock materials and a new method for rockburst proneness prediction: field demonstration," *Journal of Petroleum Science and Engineering*, vol. 205, Article ID 108997, 2021.